



VCU

Virginia Commonwealth University
VCU Scholars Compass

Theses and Dissertations

Graduate School

2011

SYNTHESIS OF NANOCOMPOSITES BY LASER ABLATION

STEPHEN MUTISYA

Virginia Commonwealth University

Follow this and additional works at: <https://scholarscompass.vcu.edu/etd>



Part of the [Physics Commons](#)

© The Author

Downloaded from

<https://scholarscompass.vcu.edu/etd/231>

This Thesis is brought to you for free and open access by the Graduate School at VCU Scholars Compass. It has been accepted for inclusion in Theses and Dissertations by an authorized administrator of VCU Scholars Compass. For more information, please contact libcompass@vcu.edu.

Synthesis of Nanocomposites by Laser Ablation

A thesis submitted in partial fulfillment of the requirements for the degree of Master of Science in Physics / Applied Physics at Virginia Commonwealth University.

By

Stephen M. Mutisya

B.S. in Physics

Virginia Commonwealth University, 2009

M.S. in Physics/Applied Physics

Virginia Commonwealth University, 2011

Directors:

Massimo F. Bertino, Associate Professor, Department of Physics

Dexian Ye, Assistant professor, Department of Physics

Sally Hunnicutt, Associate Professor, Department of Chemistry

Virginia Commonwealth University,

Richmond, Virginia, 23284

May 2011

Acknowledgments

Foremost, I would like to express my sincere gratitude to my advisor Dr. Bertino for the support of my study and research, for his patience, motivation, enthusiasm, and guidance. He has supported me throughout my thesis with his patience and knowledge whilst allowing me the room to work in my own way. I attribute the level of my Masters degree to his encouragement and effort.

Besides my advisor, I would like to thank the rest of my thesis committee members: Dr. Ye, Dr Ryan, and Dr. Hunnicutt for their motivation and insightful comments over my thesis paper.

My sincere thanks also go to Dr. Baski, for offering me the opportunity to pursue my physics masters here at VCU and also for providing me with insightful comments on both my thesis paper and final presentation. I would also like to thank all members of the physics faculty including Dr. Rechshkov, Dr. Ameen, Dr. Bishop, Dr. McMullen, and Dr. Jena for nourishing me with physics fundamentals and concepts. I would also like to thank the administrative staff; Janice and Evelyn for the encouragement they gave me through out my study.

Throughout my study, I was blessed with a friendly and cheerful group of fellow students. Charles Wingfield and Louis Franzel who were both part of Dr. bertino's group were not only labmates, but also like brothers to me. I am indebted to them for the much I learned from them. Also, I would like to include my fellow physics students including, Michael Foussekis, Joe Ferguson, Mary Willis, Vincent Ong, Iwona Ruchala, Swayamprabha Behera, Nahla Albarakati, Christopher Powell, Mathias Auer, Steele Parris, Andrew Willyard, Sean Kenny, Marrwa AlRreshedan, Joy McNamara, Crystalautumn Cameron, Anita Olsen, and Samantha Boyd. You were all great people who made my experience here at VCU very amazing.

Last but not the least, I would like to thank my family on the other side of the globe. Though none of the family can understand anything after this page, they have been motivating me and supporting me spiritually through out my academic life.

Table of Contents

Acknowledgments	ii
Table of Contents	iii
List of Figures	iv
Abstract	v
Chapter 1: Introduction to Materials and Techniques	1
1.1 Nanocomposite Materials.....	1
1.2 Laser Ablation	2
1.3 Dynamic Light Scattering (DLS)	3
1.4: Zeta Potential	5
1.5: Ultraviolet-Visible (UV-Vis) Spectroscopy.....	6
1.6: Transmission Electron Microscope (TEM).....	7
1.7: Enzyme Linked Immunosorbent Assay (ELISA)	7
1.8: Flow Cytometry	9
Chapter 2: Experiment and Results	11
2.1 Laser ablation set up.....	11
2.2 Ultraviolet-Visible Spectroscopy (UV-Vis) data	13
2.3 Dynamic Light Scattering (DLS) data	16
2.4 Zeta potential data	18
2.5 Transmission Electron Microscope (TEM).....	19
2.6 ELISA Data	22
2.7 Flow Cytometry Data	23
Chapter 3: Summary and Conclusions	26
REFERENCES.....	27

List of Figures

Fig. 1.1: SL312 series laser optical layout	2
Fig. 1.2: Schematic of DLS apparatus.....	4
Fig. 1.3: Principle of zeta potential measurements.	5
Fig. 1.4: Schematic of ELISA.	8
Fig. 1.5: The schematic of flow cytometry measurements.	10
Fig. 2.1: Schematic of laser ablation.....	11
Fig. 2.2: Laser-ablated gold surface for (a) 5 min., (b) 10 min., and (c) 10 min. with area measurement indicated for the laser-ablated hole.	12
Fig. 2.3: UV-Vis spectra of AuNP solution for (a) 5 min. and (b) 10 min. laser ablation.....	14
Fig. 2.4: Normalized UV-Vis spectra of AuNP solution before and after conjugation with IgE for a 5 min. laser ablation.....	15
Fig. 2.5: UV-Vis spectra of AuNP solution before and after conjugation with IgE for a 10 min. laser ablation.....	15
Fig. 2.6: DLS size distribution for Uncentrifuged IgE conjugated gold showing bimodal size distribution for free IgE (left) and conjugated nanoparticles (right).	16
Fig. 2.7: Size distribution of centrifuged Au-IgE and Au colloids together with their mean hydrodynamic size and the standard deviation.....	17
Table 2.1: Zeta potential results for Au nanoparticles and Au_IgE nanoparticles.	18
Fig. 2.8: TEM micrograph (a) and corresponding size distribution histogram (b) for Au-IgE laser ablated for 5 min.....	20
Fig. 2.9: TEM micrograph (a) and corresponding size distribution histogram (b) for Au-IgE laser ablated for 10 min.....	21
Fig. 2.10: ELISA data for the concentration of supernatant's IgE after IgE-Au centrifugation...	23
Fig. 2.11: Flow cytometry data for cytokine (TNF) production by IgE activated mast cells.	24
Fig. 2.12: Flow cytometry data for cytokine (IL-6) production by IgE activated mast cells.....	25

Synthesis of Nanocomposites by Laser Ablation

By Stephen Mutisya

A thesis submitted in partial fulfillment of the requirements of the degree of Master of Science at Virginia Commonwealth University, 2011.

Major Director: Massimo F. Bertino, Associate Professor, Department of Physics

Abstract

Immunoglobulin E (IgE)-conjugated gold nanoparticles were produced via *in situ* conjugation of gold nanoparticles with immunoglobulin E by laser ablation of Au in a liquid solution. The colloidal stability and the size distribution of the resulting bio-nanoconjugates were examined with UV-Visible spectroscopy (UV-Vis), dynamic light scattering (DLS), and transmission electron microscopy (TEM). These techniques showed that the Au nanoparticles in aqueous solutions were highly monodispersed spherical particles with a very narrow size distribution. The particles net diameter using TEM, was found to be $D_5=3.8\pm 0.9\text{nm}$ and $D_{10}=4.7\pm 1.3\text{nm}$ while the hydrodynamic diameter obtained with DLS was found to be $D_{h5}=171\pm 12\text{nm}$, $D_{h10}=164\pm 18\text{nm}$ for 5min and 10min laser ablation time respectively. Enzyme-Linked immunosorbent Assay (ELISA) and flow cytometry measurements of the conjugates confirmed that the gold-bound protein remained biologically active, thus paving the way for the application of these nanoparticles in immuno-diagnostics, particularly in tumor-targeted drug delivery.

Chapter 1: Introduction to Materials and Techniques

1.1 Nanocomposite Materials

Nanoparticulate materials have recently become increasingly popular due to their wide potential applications in the optical, electronic, and medical fields. This is basically due to their unique optical and size dependent properties which can easily be altered by changing the size, shape, and concentration of the nanoparticles. Nanoparticles have particularly attracted intense scientific interest in medical diagnostics.¹ Bio-conjugated nanoparticles have become very important analytical tools with emerging biological and medical applications such as invention of new drugs, drug delivery vehicles, diagnostics, and in cellular imaging. The current conventional method of synthesizing bio-conjugated nanoparticles involves chemical synthesis of the nanoparticles followed by subsequent bio-functionalization with biomolecules. Although nanoparticles can be produced relatively simply by chemical reduction method, it is probable that the surface of these nanoparticles is likely to be contaminated with the by-products of the reaction such as reducing agents and anions, which can interfere with the stabilization and functionalization with biomolecules. Overall, chemically prepared bio-conjugated nanoparticles are often not ideal for medical applications due to their toxicity which results from the chemical precursors and additives during their synthesis.

In situ conjugation of nanoparticles with biomolecules by laser ablation is a highly promising method for the efficient production of functional nanoparticles. This laser-ablation-based *in situ* conjugation is a rapid and one-step production method which produces bio-conjugated nanoparticles free of contaminants.² In this study, gold nanoparticles were successfully conjugated with Immunoglobulin E (IgE) by laser ablation. Although labeling of colloidal gold with aptamers such as DNA by laser ablation has been studied before,¹ the biological activities of complex molecules such as IgE nanoparticles have not been examined.

The main objective of this research was to synthesize, characterize, and most importantly study the biological activities of gold and IgE nanobioconjugates. The latter was done by measuring the binding and cytokine responsiveness of the gold-conjugated IgE on mast cells and as well as by performing Enzyme-Linked Immunosorbent Assay (ELISA).

1.2 Laser Ablation

Ultra short pulse lasers are designed to generate a light pulse lasting on the order of nanoseconds (10^{-9} s), picoseconds (10^{-12} s), or femtoseconds (10^{-15} s) and having very high output power. They are generated by a technique known as Q-switching which allows the energy stored in the laser gain medium to be released in a short burst once it is built up to certain high levels. Ultrashort pulse laser ablation is very advantageous since the target material is heated up to the vaporization temperature in a very short time. This leads to localization of the laser energy at a specific region of interest because the energy has no time to dissipate into the deeper parts of the material. For this study, we employed a laser (EKSPLA 312G) which produces 150 picosecond pulses with wavelength of 532 nm and an energy of up to 40 mJ/pulse. In our laser system, a 5 nanosecond pulse is produced by a Q-switched YAG laser, as shown in Fig. 1.1.

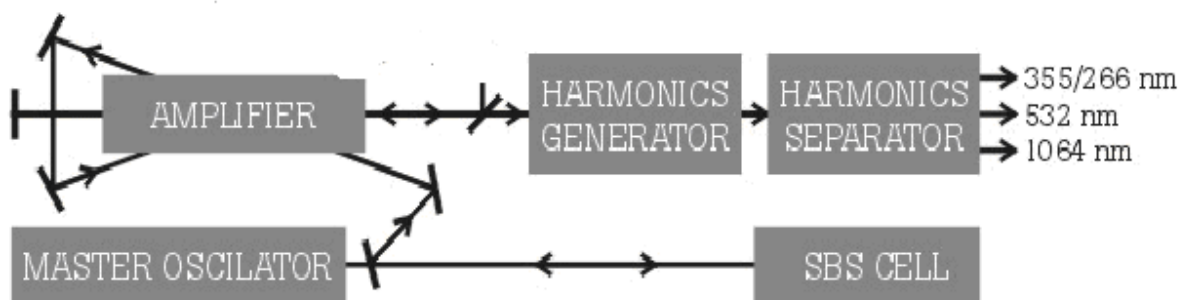


Fig. 1.1: SL312 series laser optical layout

The pulse from the YAG laser is then compressed during backward-stimulated Brillouin scattering (SBS). The pulse compressor consists of an optical guiding system and an SBS cell

filled with Carbon Tetrachloride(CCl_4) liquid. The linearly polarized light pulse from the master oscillator is focused into the SBS-cell utilizing lens in a way to compress the pulse via the SBS process. After SBS compression, the pulse is directed to a multi-pass power amplifier system which is based within the laser chamber and contains a Nd:YAG rod pumped by two plasma flash lamps providing high-energy pulses.³ Thermocontrolled harmonics generators, based on angle-tuned Potassium Dideuterium Phosphate and Potassium Dihydrogen Phosphate crystals double and triple the initial laser frequency of 1064 nm down to 532 nm and 366 nm respectively. The harmonic separation optics have dichroic mirrors which separate the fundamental and harmonic pulses with each wavelength having a separate output port.⁴

1.3 Dynamic Light Scattering(DLS)

Also known as Photon Correlation Spectroscopy (PCS). DLS is a technique designed for measurements of sizes, diffusion coefficients, viscosities, and molecular weights of dispersed sub-micron particles suspended in a liquid medium. The technique was established by the Royal Radar Establishment, Malvern UK in 1970.⁵ In DLS, a solution is illuminated with a monochromatic light beam. The solution contains spherical particles and Brownian motion causes a Doppler shift when the light impinges upon the moving particle, changing the wavelength of the incoming light. This technique monitors the time dependence of the intensity of light scattered by the medium and the rate at which the intensity fluctuates about its average value. The fluctuation rate depends upon the rate at which the scattering elements move in the solution, and is characterized by an apparent diffusion coefficient, D . Measuring the diffusion coefficient of the particles and using the correlation function, the sphere size distribution can be computed.⁷

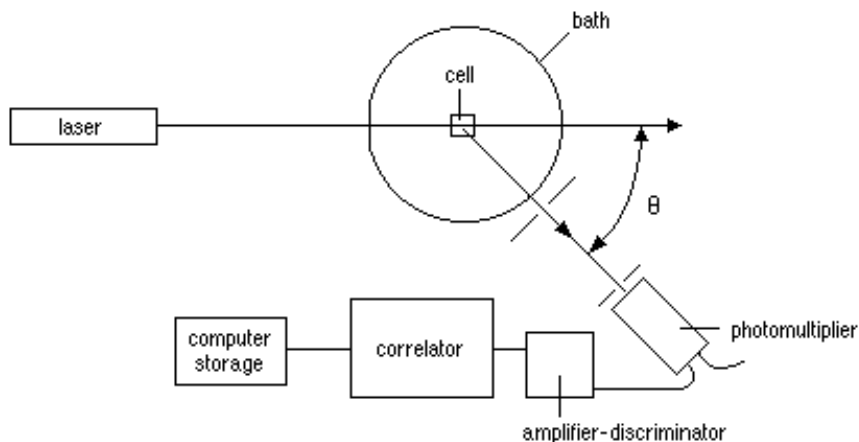


Fig. 1.2: Schematic of DLS apparatus [Adapted from ref⁶]

The decay of the autocorrelation is described by an exponential decay function $G(\tau)$ which relates the autocorrelation to the diffusion coefficient D and the measurement vector K :

$$G(\tau) \propto e^{-2DK^2\tau}$$

$$K = \frac{4\pi\eta}{\lambda} \sin\left(\frac{\theta}{2}\right)$$

where η = refractive index of the solution, λ = laser wavelength, and θ = scattering angle.

By fitting the points of autocorrelation to the function $G(\tau)$, the diffusion coefficient D can be measured and related to an equivalent sphere of diameter d using the Stokes - Einstein equation:

$$D = \frac{k_B T}{3\pi\eta d}$$

where η = diluent viscosity (water = 8.94×10^{-4} kg/(ms)), T = temperature (K) (room temp = 298 K), k_B = Boltzmann constant (1.3807×10^{-23} J/K), and d = sphere diameter (m).

The sphere diameter, d , gives the hydrodynamic diameter of the colloidal nanoparticles.

1.4: Zeta Potential

The Zetasizer potential measurement instrument calculates the zeta potential by determining the electrophoretic mobility and then applying the Henry equation.⁷ The electrophoretic mobility is the velocity of dispersed particles under the influence of electrical field. It is obtained by performing an electrophoresis experiment on the sample and measuring the velocity of the particles using Laser Doppler velocimetry. The development of a net charge at the particle surface affects the distribution of ions in the surrounding interfacial region, resulting in an increased concentration of counter ions (ions of opposite charge to that of the particle) close to the surface. Thus, an electrical double layer exists around each particle. The liquid layer surrounding the particle exists as two parts; an inner region known as Stern layer, where the ions are strongly bound and an outer, diffuse region where they are less firmly attached. The Zeta potential is the potential that exists at this boundary within the diffuse layer where the ions and particles form a stable entity.⁷

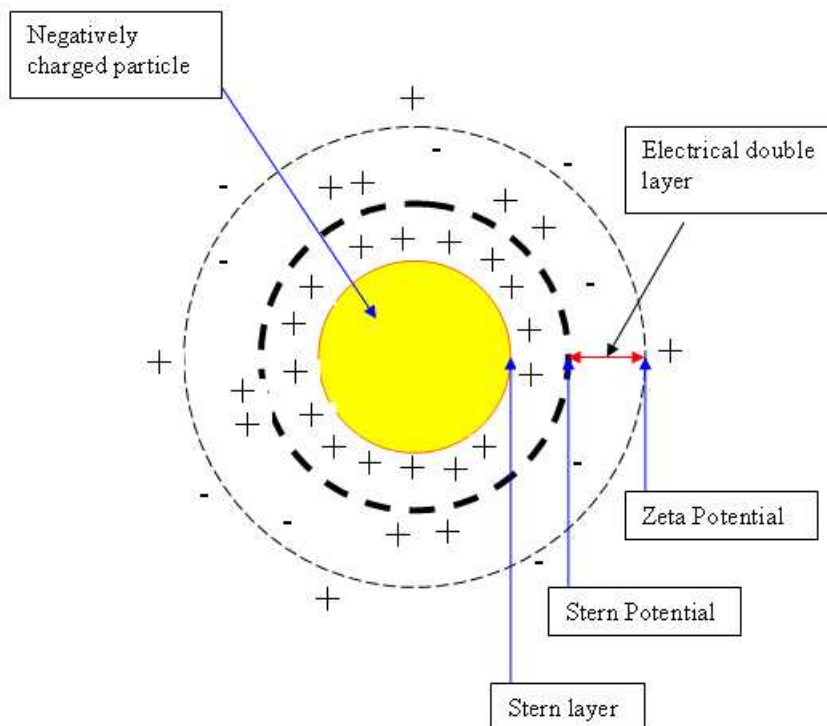


Fig. 1.3: Principle of zeta potential measurements [adapted from ref. ⁸]

The magnitude of the zeta potential gives an indication of the potential stability of the colloidal system. If all the particles in suspension have a large negative or positive zeta potential then they will repel each other and there will be no tendency to aggregate. However, if the particles have low zeta potential values then there is no force to prevent the particles coming together and flocculating. The general dividing line between stable and unstable suspensions is generally taken at either +30mV or -30mV.⁵

1.5: Ultraviolet-Visible (UV-Vis) Spectroscopy

Ultraviolet-visible (UV-Vis) spectroscopy is a technique commonly used to analyze compounds in the ultraviolet (UV) and visible (Vis) regions of the electromagnetic spectrum. It is usually used to measure absorbance of a material at specific wavelengths. UV-Vis is especially useful to characterize noble metal nanoparticles. Noble metal nanoparticles are characterized by a strong surface absorption band called surface plasmon which is classically due to collective oscillations of the conduction electrons in response to electromagnetic excitation. UV-Vis spectroscopy was also used to test the stability of the colloidal nanoparticles by comparing both the colloidal gold and the IgE stabilized gold nanoparticles surface plasmon peak. The absorption spectra were also used to determine the concentration of the gold nanoparticles by employing the Beer's law relation;

$$A = \epsilon bc$$

where Absorbance, A , is given by $A = \log(P_0 / P)$, P_0 and P are reference and sample light beams, respectively, ϵ = molar absorptivity coefficient ($M^{-1}cm^{-1}$), b = path length of sample (cm), and c = concentration of colloidal particles (M).

1.6: Transmission Electron Microscope (TEM)

This technique makes use of an electrons beam, that is transmitted through a very thin grid containing the sample of interest. The image is focused onto a fluorescent screen or detected by a CCD camera from electrons which are transmitted through the specimen. The small electrons' de Broglie wavelength makes high resolution imaging possible with TEM. The TEM analysis was used to study the size distribution of the gold nanoparticles. The Equipment used was a Carl Zeiss Libra 120 plus Transmission Electron microscope operating at 120kV, and equipped with a Gatan Multiscan CCD camera. The samples were prepared by adding a drop of the solutions on a grind of copper which covered with a carbon film on one side and allowing the sample to dry overnight under room temperature.

1.7: Enzyme Linked Immunosorbent Assay (ELISA)

This is an immunochemical technique which provides a sensitive, rapid and reliable assay for detection and quantification of antigen specific antibodies or basically to estimate biological parameters precisely. The test involves an enzyme which consists of a protein that catalyzes a biochemical reaction and also an antibody or antigen which is usually an immunologic molecule. The actual test consists of a plate which is coated with the antigen of a specific antibody. This antigen binds with the specific primary antibody on a given plasma sample. A secondary antibody which is enzyme-linked is introduced and binds with the primary antibody which is already bound to the antigen. This secondary antibody releases the attached enzyme when it binds itself with the primary antibody and then a colorless developing solution is added. The color of the developing solution changes once it reacts with the enzyme attached on the secondary antibody. The intensity of the color change is quantified with a spectrometer at 450nm. In our case, the quantity of bound enzyme varies directly with the concentration of IgE in the sample of interest. Thus the absorbance at 450nm is the measure of the concentration of IgE in the sample which is directly proportional to the

color intensity of the developing solution. A standard curve which is corrected for sample dilution is used to quantify the IgE present by interpolation.

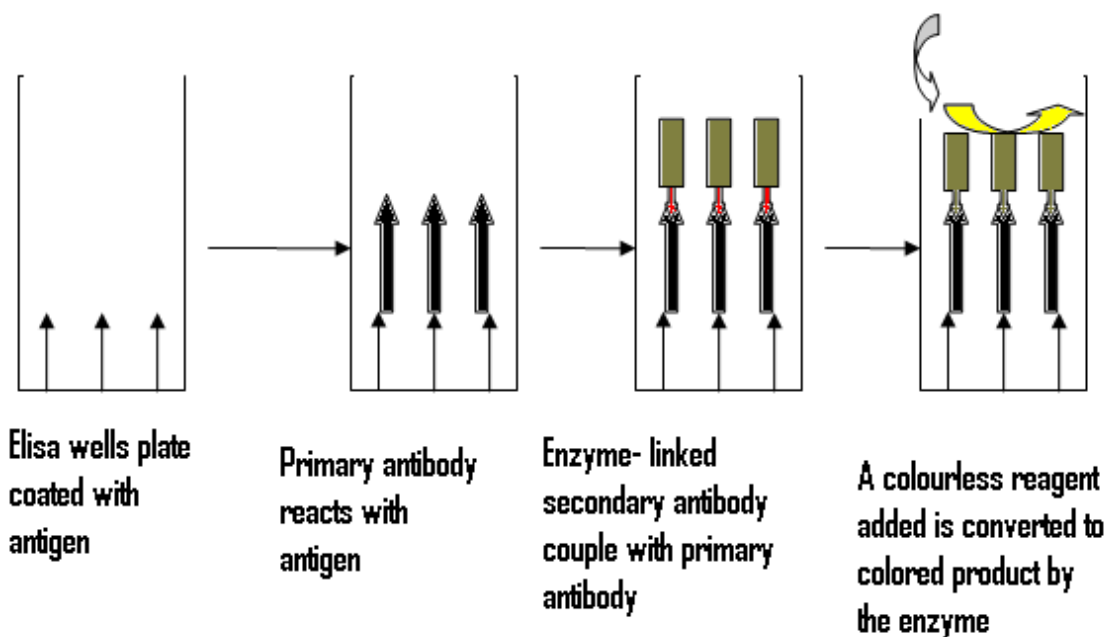


Fig. 1.4: Schematic of ELISA.

A test sample of gold conjugated IgE was prepared as described. The concentration of the IgE in the conjugate was 3 $\mu\text{g/ml}$. A plate consisting of polystyrene microtiter wells were prepared by washing with a wash solution of 50mM Tris, 0.14M NaCl, 0.05% Tween 20 and coating it with a 0.05M borate saline buffer. Biotin label anti-IgE antibodies were adsorbed to the surface of polystyrene microtitre wells. Gold-conjugated IgE solution was then added to the anti-IgE antibodies immobilized on the wells and then incubated. Any active IgE present in the IgE coupled gold conjugate will combine with the label anti-IgE antibody on the well. The well is then washed with de-ionized water to remove any unbound test sample. A secondary anti-IgE antibody conjugated with enzyme horseradish peroxidase is added. This enzyme-labeled antibody will bind immunologically to the IgE on the well and it result in IgE molecules being sandwiched between the anti-IgE antibodies and the enzyme-linked antibodies. The unbound secondary antibody is washed with de-ionized water and then a solution of Tetramethylbenzidine is added and incubated for several min. This chromogenic

substrate reacts with the enzyme bound to the secondary antibody leading to development of blue color. Sulfuric acid was then added to stop the TMB reaction resulting to yellow color. A microtiter plate reader was used to read the absorbance of the yellow color at a wavelength of 450nm. The absorbance was then compared with the standard curve to obtain the corresponding IgE concentration.¹

1.8: Flow Cytometry

Flow cytometry is a laser-based technique which measures characteristics of biological particles. The cells of interest are labeled with fluorescent markers such as dyes and forced out of a small nozzle in a liquid jet stream. Fluorescent detectors are used to measure emitted light from the fluorescently-labeled cells as they become forced out of a small nozzle in a liquid jet stream. A beam of monochromatic light is directed onto the stream where each of the suspended particles scatters some of the light beam. A fluorescence detector detects the scattered light and the brightness fluctuations which correlates with the cell volume.

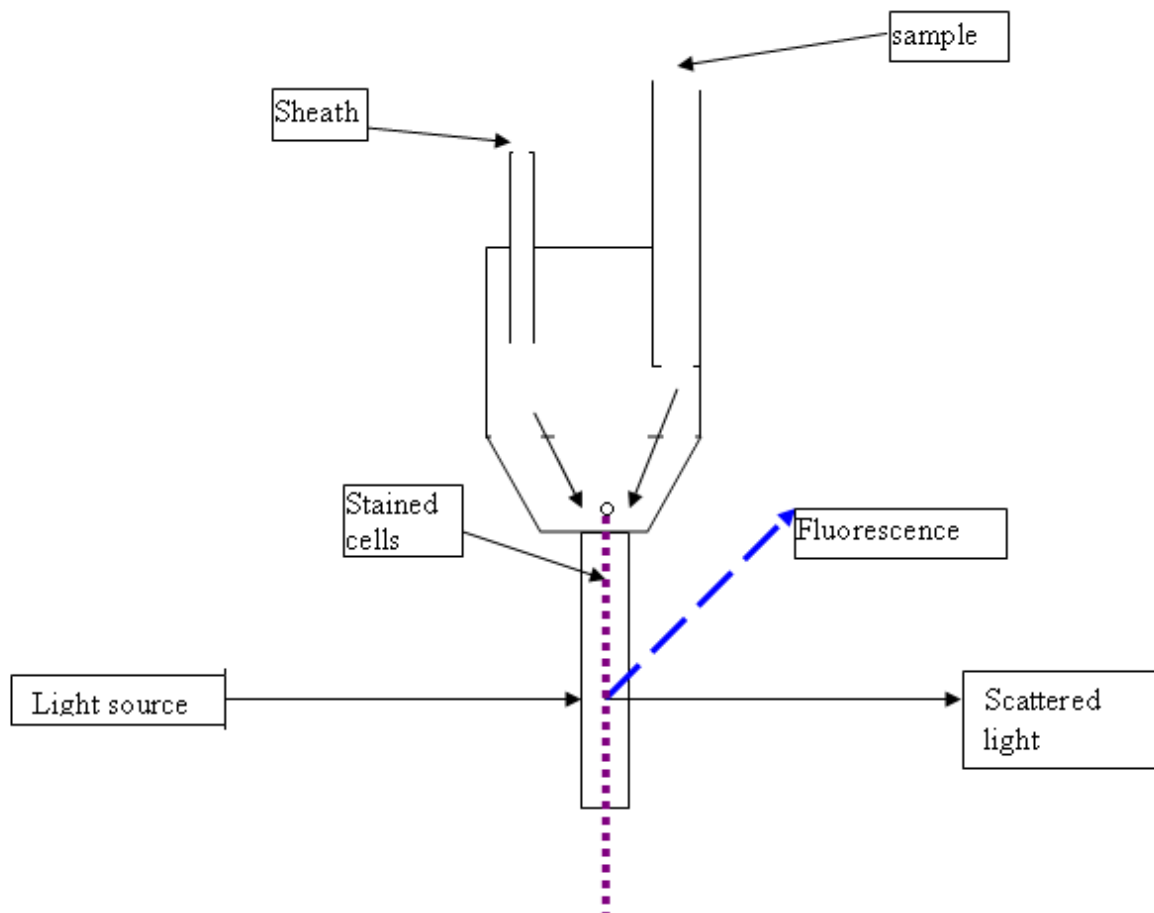


Fig. 1.5: The schematic of flow cytometry measurements (Adapted from ref. ¹²).

Chapter 2: Experiment and Results

2.1 Laser ablation set up

The set up for the laser ablation of gold nanoparticles was as shown in fig. 2.1. The gold target was bombarded at 10% of the maximum laser power energy to limit the denaturation of the biomolecules and also to prevent drilling through the gold target by laser. Typically, a laser power of 4 mJ was employed. The pulse duration was 150 ps and the pulse repetition rate was of 10 Hz. Two set of samples were prepared by exposing the target gold for 5 and 10 min. The samples were immediately characterized with Ultraviolet-Visible Spectroscopy (UV-Vis), Dynamic light scattering (DLS), Transmission Electron Microscope (TEM) and Enzyme Linked Immunosorbent(ELISA). A typical crater made by the picosecond laser on the gold target was measured with a Nikon Eclipse LV100D-U optical microscope and is shown in Fig 2.2.

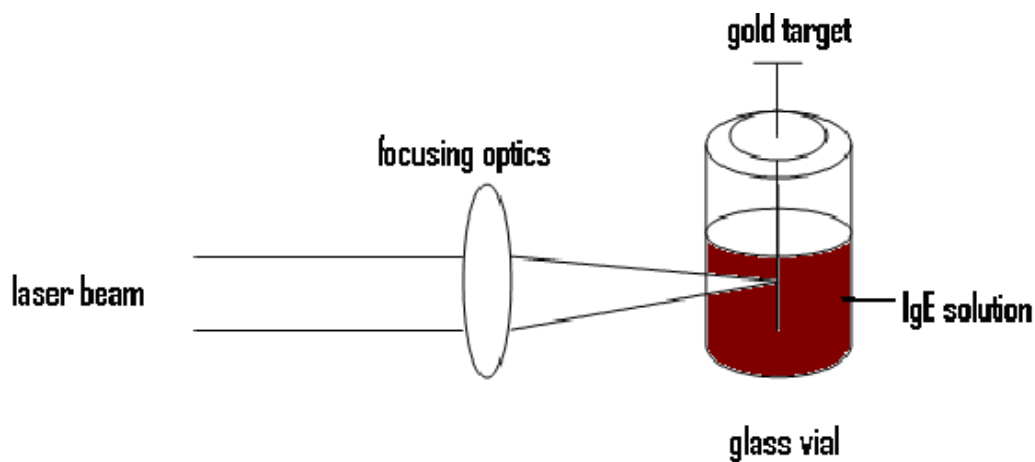


Fig. 2.1: Schematic of laser ablation.

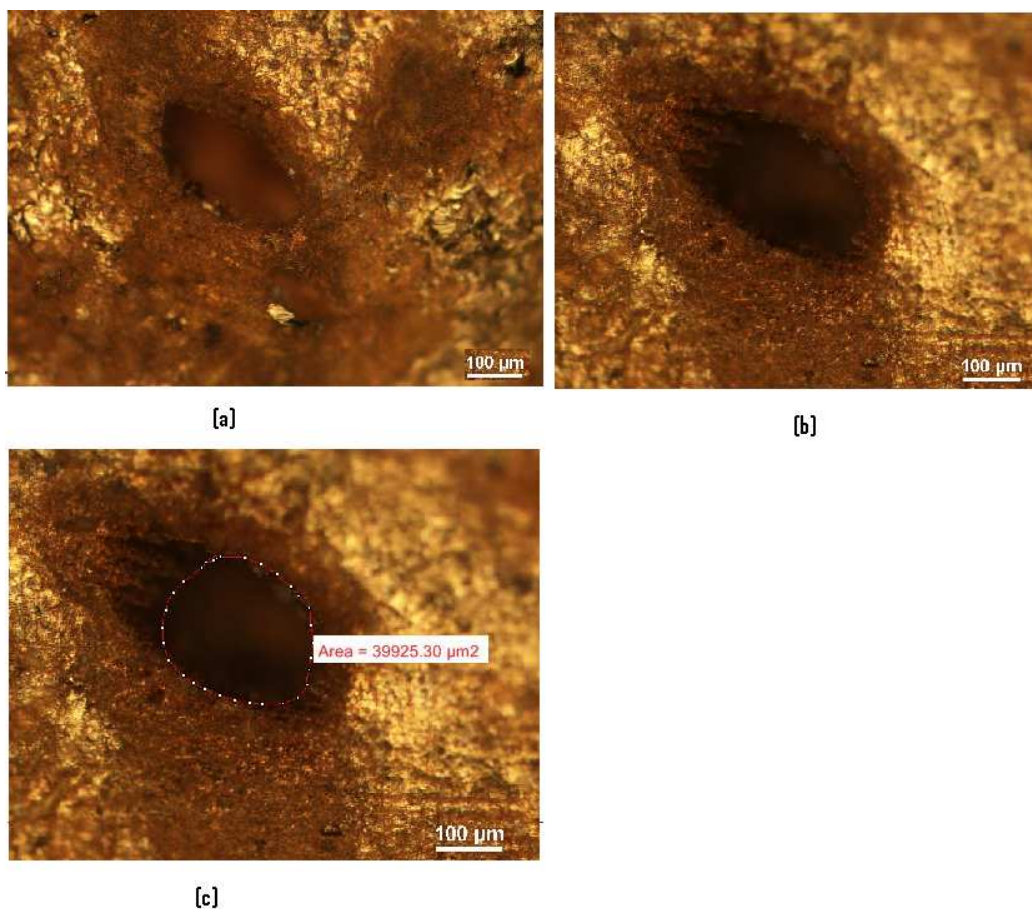


Fig. 2.2: Laser-ablated gold surface for (a) 5 min., (b) 10 min., and (c) 10 min. with area measurement indicated for the laser-ablated hole.

As seen in Fig. 2.2, the crater profiles were not perfectly circular. This was due to the change of the laser beam's spot position on the target surface during ablation, which was as a result of the loose rod's holder or a perturbation of the liquid layer near the focal point leading to the change of the liquid layer refraction properties.⁹ The materials are usually vaporized as nanoparticles. As shown in Fig. 2.2, thermal effects or charred materials around the entrance of the holes are not evident, signifying that the laser energy was localized at the point of impact. This indicates that the ultra-short pulsed laser has a very limited heat-affected volume. By using the area of the ablated laser hole ($4 \times 10^{-4} \text{ cm}^3$) and the maximum energy of 4 mJ/pulse, the ablation energy was found to be 10 Jcm^{-2} per pulse, which is 10 times higher than the gold picosecond laser ablation threshold of 0.9 Jcm^{-2} .¹⁰

2.2 Ultraviolet-Visible Spectroscopy(UV-Vis) data

Since optical properties of nanoparticles are very crucial when it comes to their application in nanotechnology and more importantly in the medical field,¹¹ investigating the optical properties of the IgE-conjugated nanoparticles was very valuable. The ablation process of the gold target was accompanied by a solution color change to bright red indicating the production of small sized gold nanoparticles. Gold nanoparticles were first prepared in pure PBS solution for the quantification of their concentration. As shown by the absorption spectra in Fig. 2.3, the colloidal gold nanoparticles exhibited a broad peak at 525 nm. This peak is attributed to the localized Plasmon resonance of the gold nanoparticles. To determine the gold nanoparticles concentration, the absorption at 52 nm was determined and Beer's law was used to estimate the concentration. To determine absorbance, the absorbance at 450nm was subtracted from the value of the maximum of the Plasmon resonance at 525nm. This subtraction was found by previous work to be a reliable method to measure the concentration of the suspensions of Au NPs. The molar absorptivity coefficient of gold colloids used was $1.1 \times 10^7 M^{-1} cm^{-1}$, which is the standard value for gold nanoparticles with size in the range of 2-10 nm.¹² The path length of the square cuvette used was 1cm. Thus for particles prepared with laser ablation for 5 min. and 10min., their concentration was calculated to be $3.1 \times 10^{-9} M$ and $5.5 \times 10^{-9} M$ respectively as shown in Fig. 2.3. The normalized absorption spectra of Au and Au-IgE suspensions were reported in In figure 2.4 and 2.5,. We notice that the spectra of pure Au NPs were somewhat broader and red shifted, suggesting the presence of aggregates.

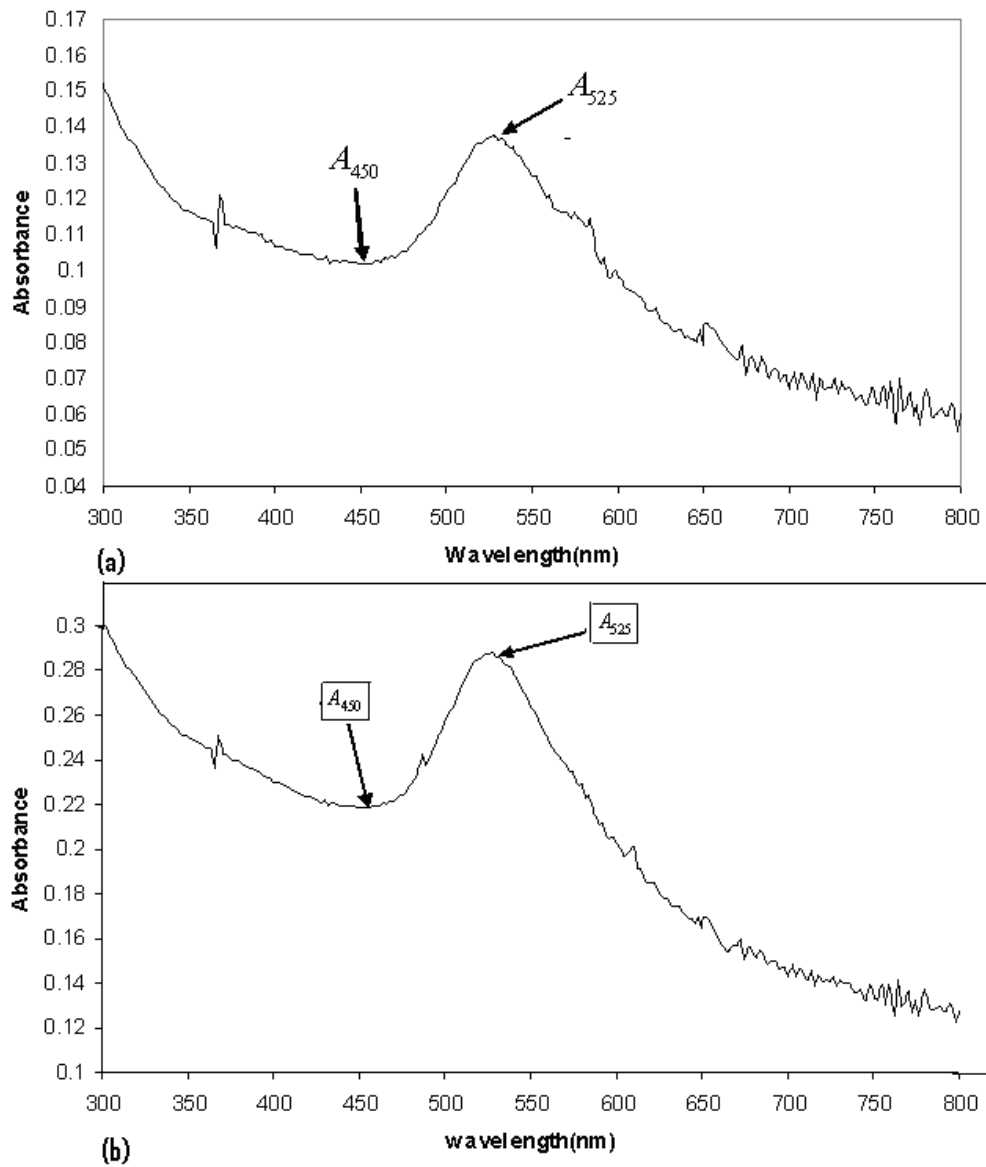


Fig. 2.3: UV-Vis spectra of Au-NP solution for (a) 5 min. and (b) 10 min. laser ablation.

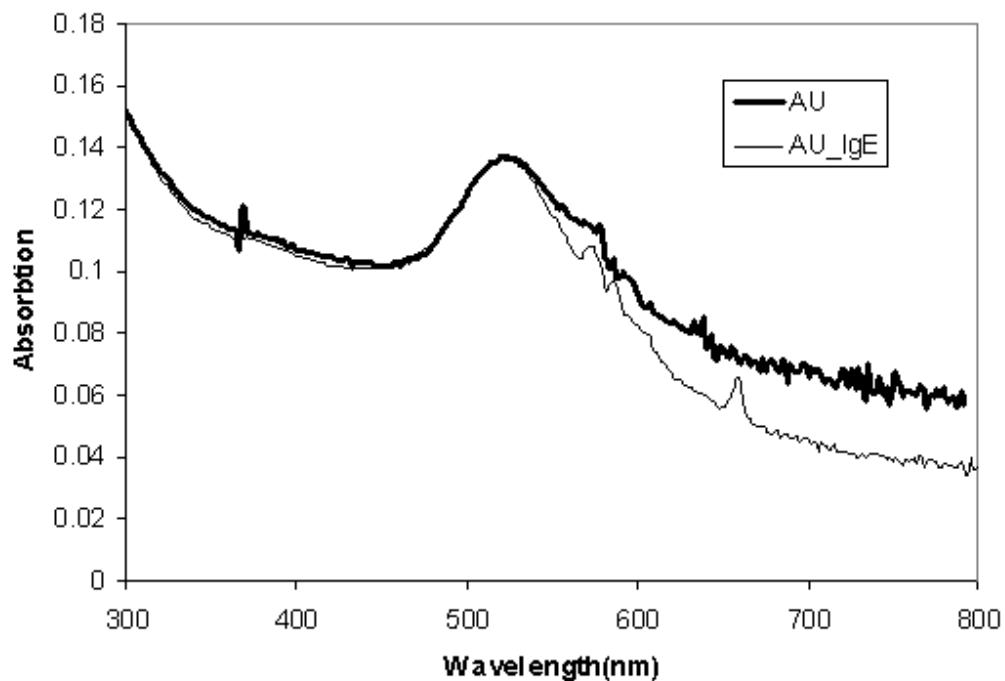


Fig. 2.4: Normalized UV-Vis spectra of Au-NP solution before and after conjugation with IgE for a 5 min. laser ablation.

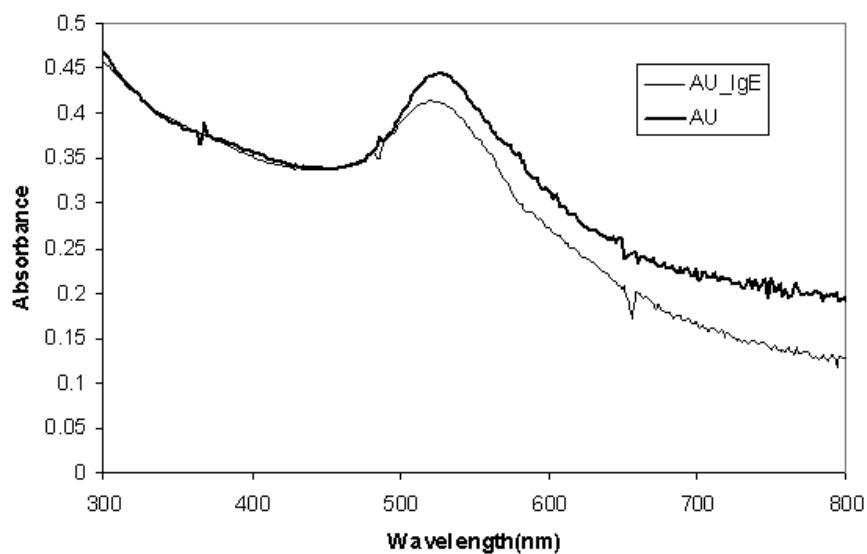


Fig. 2.5: UV-Vis spectra of Au-NP solution before and after conjugation with IgE for a 10 min. laser ablation.

2.3 Dynamic Light Scattering(DLS) data

The DLS was specifically used to analyze the hydrodynamic size distribution and the stability of the IgE conjugated gold. Analysis was done using the two sets of IgE conjugated gold samples, which were laser ablated for 5 and 10 min. Each sample was placed in a quartz cuvette and then inserted in the sample holder on the optics block of the DLS. The measurements were done in triplicate to ensure reproducibility with each measurement having 15 acquisitions. The DLS determines the hydrodynamic size by measuring the angles which an incident light beam is scattered as a function of Brownian motion of the colloidal gold particles.¹³ Uncentrifuged IgE conjugated gold samples indicated the presence of free or unbound IgE in the sample as shown in the figures below. The presence of an extra peak at 30 nm and 40 nm for IgE conjugated Au-NP, laser ablated for 5 and 10 min., respectively, which disappear after centrifugation.

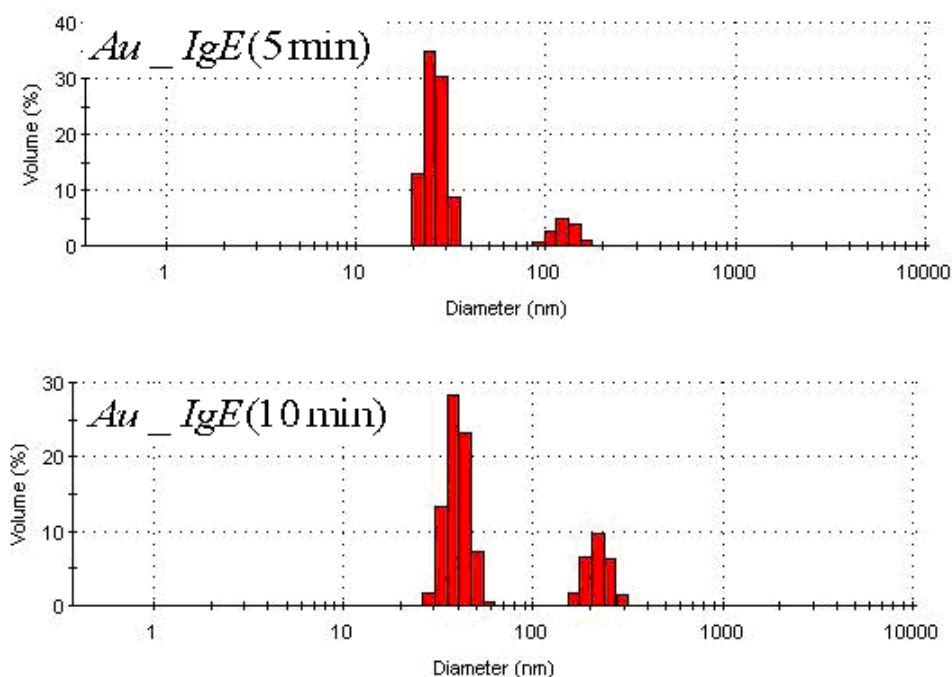


Fig. 2.6: DLS size distribution for Uncentrifuged IgE conjugated gold showing bimodal size distribution for free IgE (left) and conjugated nanoparticles (right).

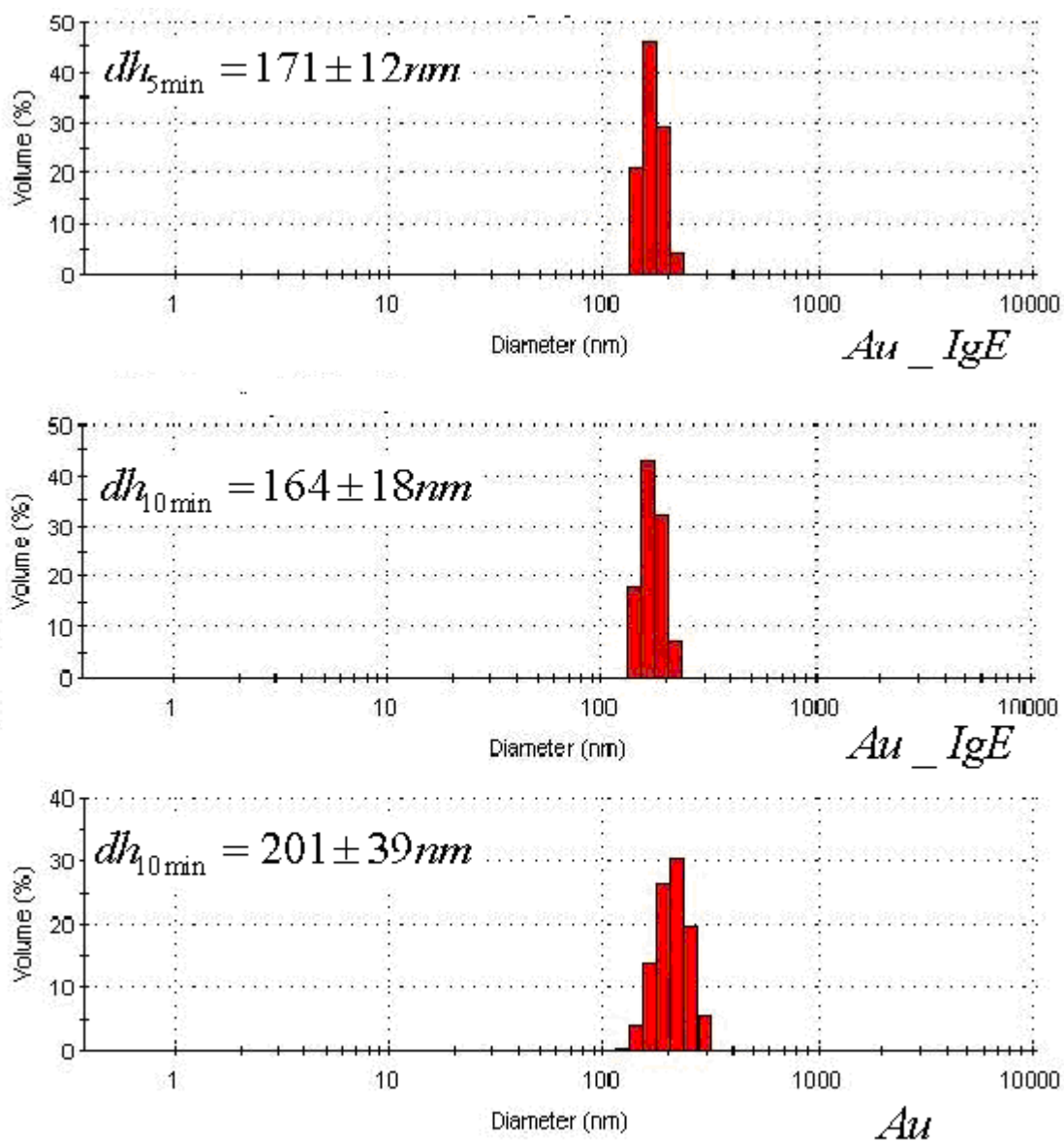


Fig. 2.7: Size distribution of centrifuged Au-IgE and Au colloids together with their mean hydrodynamic size and the standard deviation.

2.4 Zeta potential data

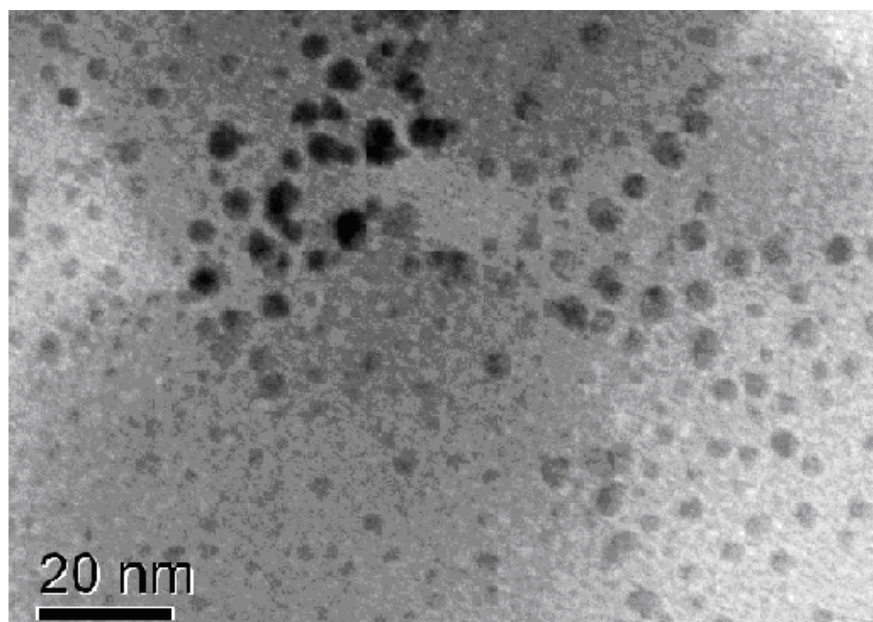
The zeta potential of colloidal gold nanoparticles is an excellent predictor of the stability of the colloids as it indicates the magnitude of the electrostatic repulsion between the nanoparticles. A low zeta potential will increase the tendency of the colloidal dispersions to coagulate because the Van der Waals forces of attraction between the colloidal particles overcomes the electrostatic repulsion.¹⁴ As stated earlier, the general dividing line between stable and unstable dispersed particles is generally taken at either +30 mV or -30 mV.¹¹ The zeta potential of non IgE conjugated gold colloids was experimentally measured to be -16.7 mV while for the IgE conjugated gold colloids was found to be -28.3 mV as shown on Data Table 2.1. This was done by averaging 4 data sets with each data set consisting of the average from ten separate acquisitions. A data set for the zeta potential from gold colloids and IgE conjugated gold colloids is as shown below in these two experimental results screen shots. Though the values of the zeta potential indicate that the colloidal gold nanoparticles were partially stable, their IgE conjugated counterparts were relatively stable. This is further illustrated by the bigger hydrodynamic diameter and a wider size distribution of unconjugated gold nanoparticles as shown on Fig. 2.7.

	Gold nps(mV)	Gold_IgE(mV)
Run 1	-22.9	-27.9
Run 2	-10.8	-31.9
Run 3	-16.3	-25.6
Mean	-16.7	-28.3

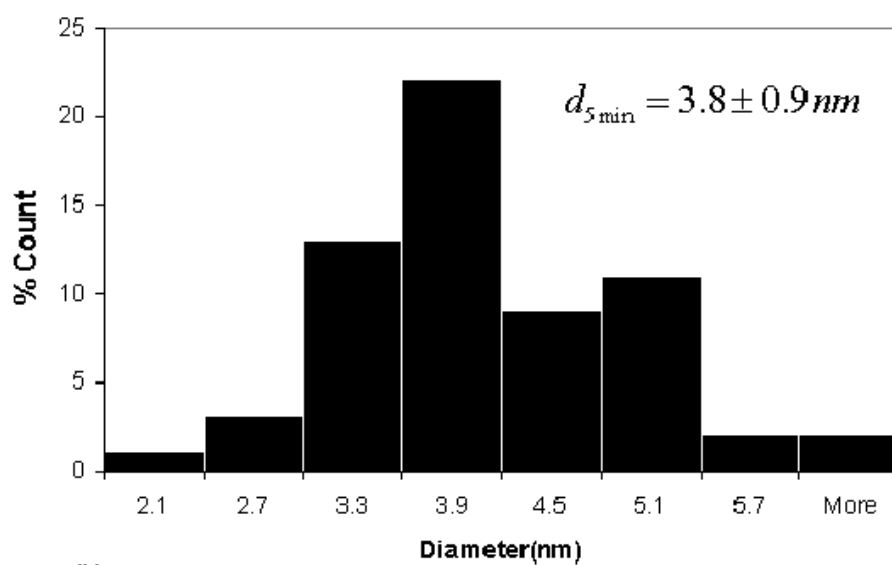
Table 2.1: Zeta potential results for Au nanoparticles and Au-IgE nanoparticles.

2.5 Transmission Electron Microscope (TEM)

TEM micrographs were used to characterize the size distribution of the gold nanoparticles. This was done by measuring the diameter of 80 particles from different sample regions. The figure below shows the size distribution of gold nanoparticles together with their corresponding TEM image for two laser ablation times. It can be seen very clearly that the spherical gold nanoparticles are approximately uniform in size. Statistical analysis of the particles size indicated that the average diameter size is $d_{5\min} = 3.8 \pm 0.9\text{nm}$ and $d_{10\min} = 4.7 \pm 1.3\text{nm}$. Since gold nanoparticles are known for their unique size-dependent properties, a narrow size distribution is advantageous for their use in advanced applications such as medical therapeutics.¹⁵



(a)



(b)

Fig. 2.8: TEM micrograph (a) and corresponding size distribution histogram (b) for Au-IgE laser ablated for 5 min..

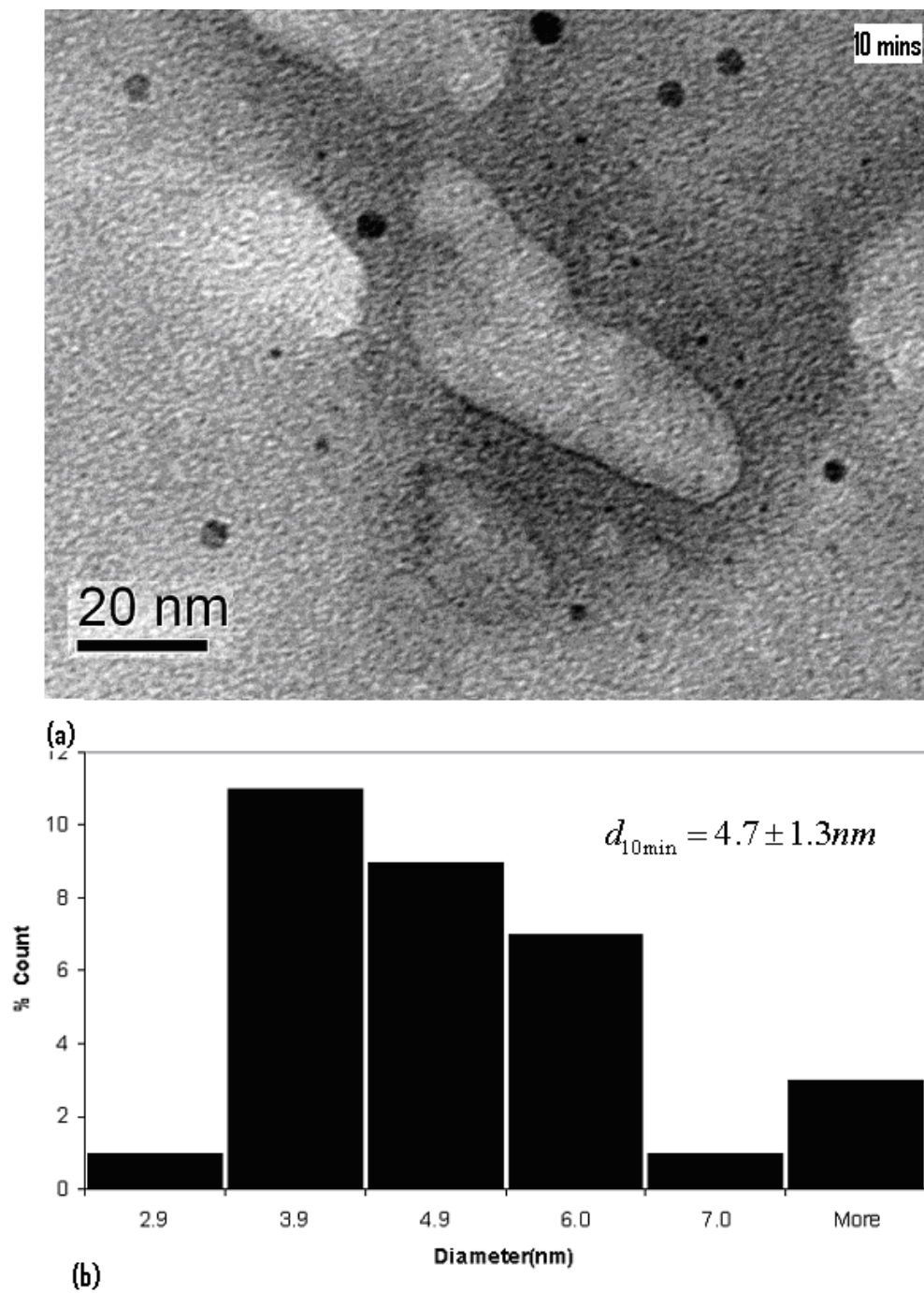


Fig. 2.9: TEM micrograph (a) and corresponding size distribution histogram (b) for Au-IgE laser ablated for 10 min..

2.6 ELISA Data

A test sample of gold conjugated IgE was prepared as described earlier. The concentration of the IgE in the conjugate was 3 ug/ml. A plate consisting of polystyrene microtiter wells were prepared by washing with a wash solution of 50 mM Tris, 0.14 M NaCl, 0.05% Tween 20 and coating it with a 0.05 M BBS coating buffer. Biotin label anti-IgE antibodies were adsorbed to the surface of polystyrene microtitre wells and then washed to remove any unbound antibodies. Gold conjugated IgE solution was then added to the anti-IgE antibodies immobilized on the wells and then incubated. Any active IgE present in the IgE coupled gold conjugate will combine with the label anti-IgE antibody on the well. The well is then washed with de-ionized water to remove any unbound test sample. A secondary anti-IgE antibody conjugated with enzyme horseradish peroxidase is added. This enzyme-labeled antibody will bind immunologically to the IgE on the well and this result to the IgE molecules being sandwiched between the anti-IgE antibodies and the enzyme-linked antibodies. The unbound secondary antibody is washed with de-ionized water and then a solution of Tetramethylbenzidine is added and incubated for several min.. This chromogenic substrate reacts with the enzyme bound to the secondary antibody leading to development of blue color. Sulfuric acid was then added to stop the TMB reaction resulting to yellow color. A microtiter plate reader was used to read the absorbance of the yellow color at a wavelength of 450nm. The absorbance was then compared with the standard curve to obtain the corresponding IgE concentration.

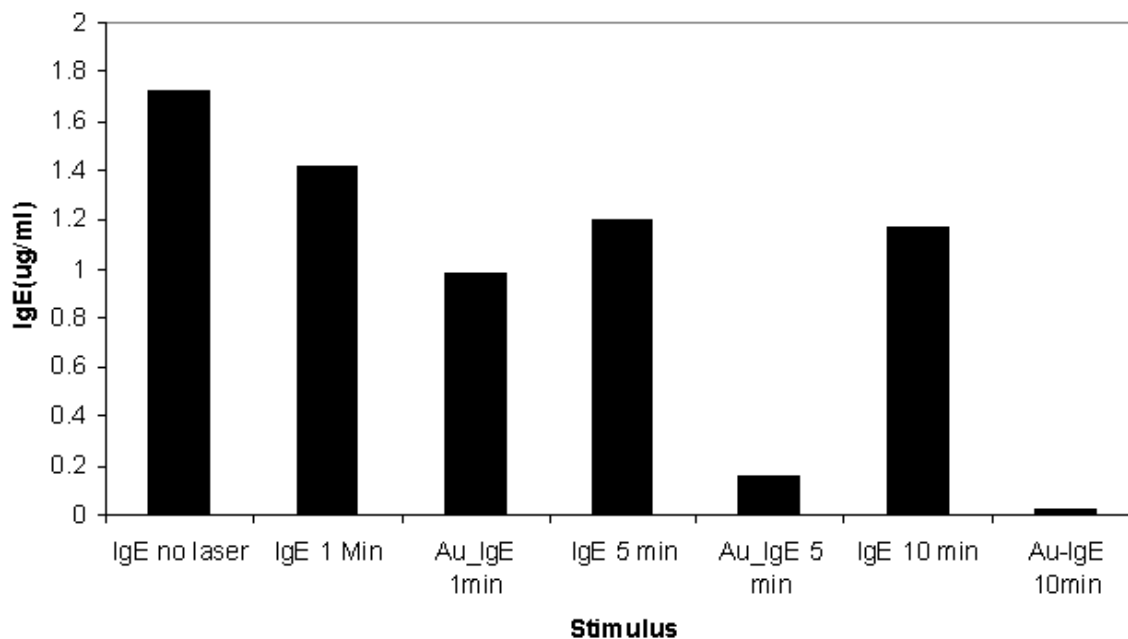


Fig. 2.10: ELISA data for the concentration of supernatant's IgE after IgE-Au centrifugation.

As shown in figure 2.10, the ELISA data shows that supernatant concentration of the centrifuged Au-IgE colloids varied with the ablation time. For 5 and 10 min. ablation time, the adsorption of IgE molecules on to the gold surface was relatively high which was indicated by the high relative difference between the laser treated IgE solution and the Au-IgE solutions laser treated for the same time. The data also indicates that, the variation of the concentration of untreated IgE and laser treated IgE was minimal. This is a proof that the laser energy does not denature the protein by high magnitude.

2.7 Flow Cytometry Data

The flow cytometry technique was used to determine the concentration of the cytokine produced by IgE induced mast cells because only biologically active IgE that is adsorbed on the surface of the gold nanoparticles is known to activate the mast cells. The concentration of the biologically active IgE can be approximated from the amount of cytokine produced by the mast cells by comparing it with calibrated standards. In this assay, Interleukin-6 (IL-6) and Tumor Necrosis Factor (TNF) which are both types of cytokine produced by activated mast

cells were analyzed and the results presented in figure 2.11 and 2.12 respectively. The flow cytometry data shows that Au-IgE conjugates does in fact bind with the mast cells but at a lower density than untreated IgE. This could be due to the actual amount of IgE adhering to the gold, which was approximated at 1-5%.

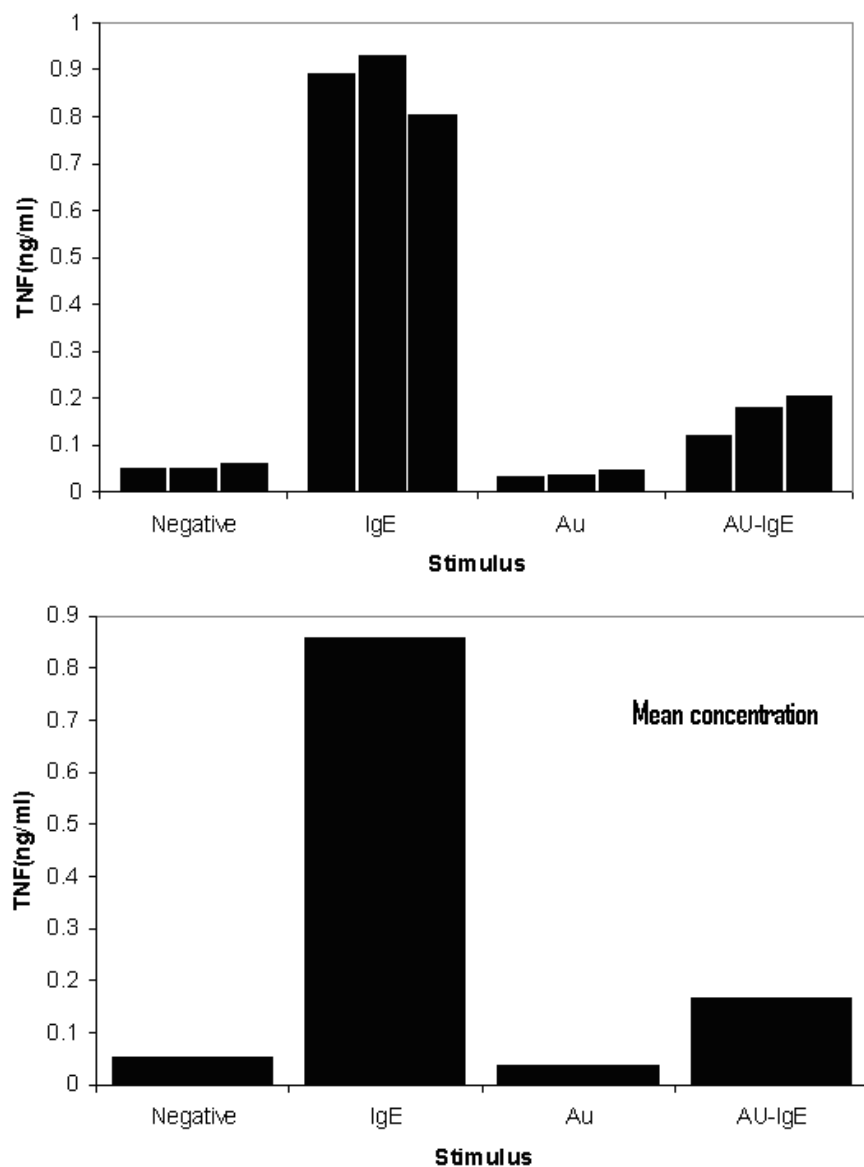


Fig. 2.11: Flow cytometry data for cytokine(TNF) production by IgE activated mast cells.

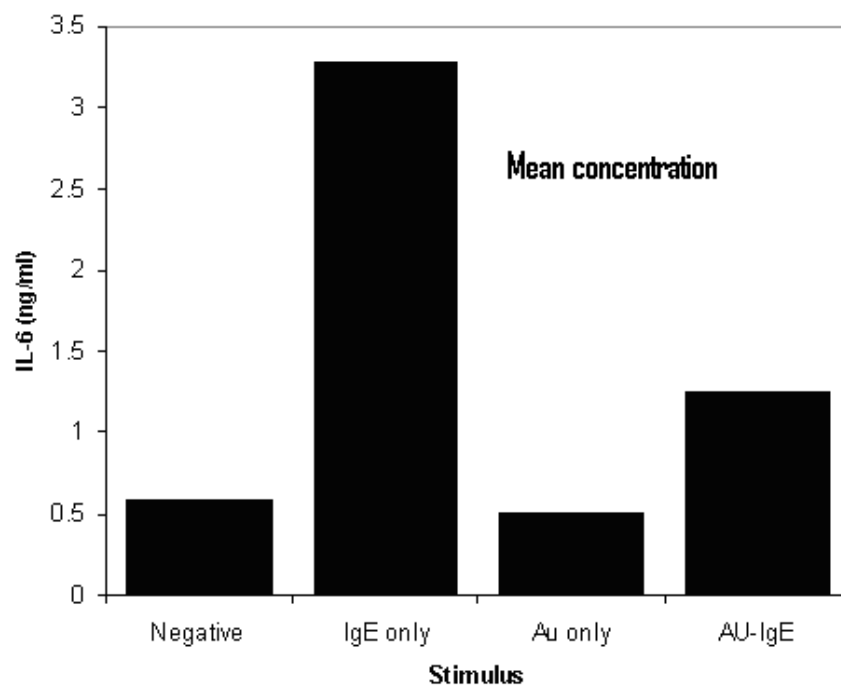
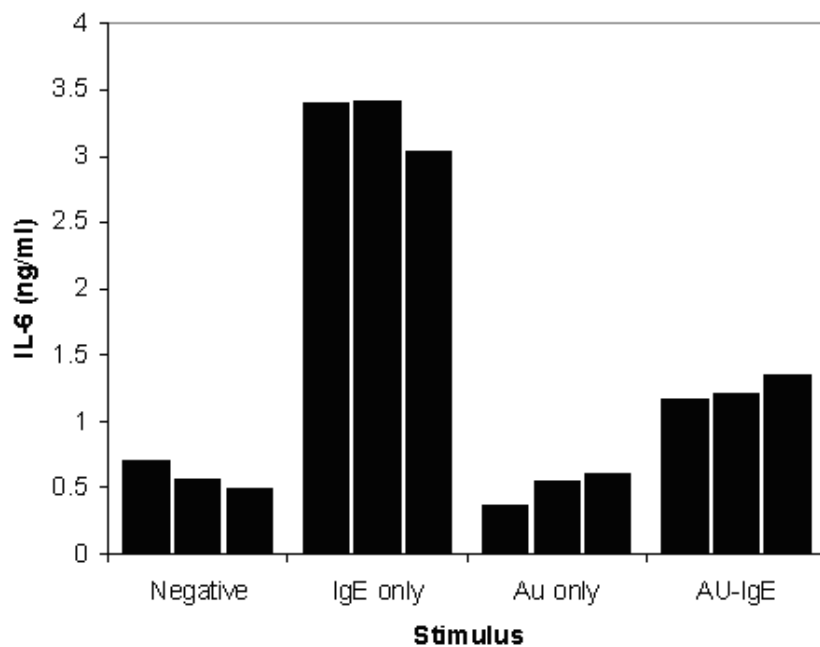


Fig. 2.12: Flow cytometry data for cytokine(IL-6) production by IgE activated mast cells.

Chapter 3: Summary and Conclusions

Adsorbing biomolecules to a metal surface such as that of gold is a challenging process which depends on the colloidal stability, shape, size, and isoelectric point of the biomolecule, and with the pH of the suspending medium. Synthesis by laser ablation of toxic-free IgE conjugated gold nanoparticles which can successfully be applied in targeting cancer drugs was explored in this study.

The IgE conjugated Au NPs were found to be;

Small with a very narrow size distribution

-Hydrodynamic Diameter (DLS); $D_{h5}=171\pm 12\text{nm}$, $D_{h10}=164\pm 18\text{nm}$

-NPs net size (TEM); $D_5=3.8\pm 0.9\text{nm}$, $D_{10}=4.7\pm 1.3\text{nm}$

Biologically active

-Positive ELISA results for IgE adsorbed on the Au-NPs surface.

-Positive results for Mast cell activation Assay

Stable colloids

-No evidence of aggregation using Zeta potential, DLS, TEM, and UV-Vis analysis.

More techniques such as the X- Ray Photon Spectroscopy can be further used to characterize the IgE conjugated gold. With this technique, we can determine if it is the carboxylic or amine sites of the IgE molecule binding to the gold. A shift in the peak of either of the two indicates the group which is binding to the gold surface. Since, the synthesis and characterization of the IgE conjugated gold was done at room temperature, may be working at 32°C (body temperature), can further determine if the biomolecules still remains adsorbed on the gold surface.

REFERENCES

-
- ¹ Johanna, W.; Svea P.; Frank S.; Thomas, S.; Stephan, B. *J. Biotechnol.* **8**,21 (2010).
- ² Andrei, V.; Michel, M. *J. Jphotochem.* **3**, 183 (2006).
- ³ Ingcrys, 2000, *Operators manual for EKSPLA SL300 series Laser*, EKSMA Group Company, United Kingdom.
- ⁴ Harilal, S.; *J. Appl.Chem*, **102**,123 (2007).
- ⁵ Nowakowski,A.; *Computer simulation and experimental investigation of laser beam interaction with metals*, MS Thesis, Worcester Polytechnic Institute,Worcester, MA, 1990.
- ⁶ Harding, S.; Jumel, K. (2001). *Current protocols in protein science*. Retrieved march 2011 from WILEY online library.
- ⁷ Smallenburg, F.; Boon, N.; Kater,M.; Dijkstra,M.; Roij, R. *J. Chem. Phys.* **134**, 074505 (2011)
- ⁸ Malvern Instruments, 2004, *Zetasizer Nano series user Manual*, Worcestershire, Emerald Group publishing LTD.
- ⁹ Meunier, M.; Kabashin. A.; Sacher, E.; *Appl. Phys. A.* **80**, 753 (2005).
- ¹⁰ Pan, Y.; Yang, W.; Yimin, Mo.; *AMR.* **189**.3759 (2011)
- ¹¹ Wolfgang,H.; Nguyen, T.; Aveyard, J.; Ferning, G. *Anal. Chem.***79**, 4215 (2007)
- ¹² Grogan, W.M. and Collins, J.M. *Guide to Flow Cytometry Methods*, Marcel Dekker (1990).
- ¹³ Weinreich, D.; Goia, D.; Pavel, N.; Mclaughlin, R.; Tamarkin, L.*Drug Delivery.* **11**. 169 (2004).
- ¹⁴ Schatzel, K. *Appl. Phys. B.* **42**, 193-213 (1987).
- ¹⁵ Jiao, Y.; Pan, W.; Huang, S.; Chen, S.; Meng, F. *ChemPhysChem.* **5**, 68 (2004).